JGR Planets

RESEARCH ARTICLE

10.1029/2021JE006832

Key Points:

- Low impact shock with proposed impact melt influences Al,Si order of plagioclases
- Grinding of rocks leads to modal changes of the minerals
- Potential plagioclases with reduced degree of Al,Si order on the surface of Mercury

Correspondence to:

M. P. Reitze,
maximilan.p-reitze@uni-muesnter.de

Citation:

Reitze, M. P., Weber, I., Morlok, A., Hiesinger, H., Bauch, K. E., Stojic, A. N., & Helbert, J. (2021). Mid-infrared spectroscopy of anorthosite samples from near Manicouagan Crater, Canada, as analogue for remote sensing of Mercury and other terrestrial solar system objects. *Journal of Geophysical Research: Planets*, *126*, e2021JE006832. https://doi.org/10.1029/2021JE006832

Received 25 JAN 2021
Accepted 1 JUL 2021

Mid-Infrared Spectroscopy of Anorthosite Samples From Near Manicouagan Crater, Canada, as Analogue for Remote Sensing of Mercury and Other Terrestrial Solar System Objects

Maximilian P. Reitze[1], Iris Weber[1], Andreas Morlok[1], Harald Hiesinger[1], Karin E. Bauch[1], Aleksandra N. Stojic[1], and Jörn Helbert[2]

[1]Institut für Planetologie, Westfälische Wilhelms-Universität (WWU), Münster, Germany, [2]Institut für Planetenforschung, Deutsches Zentrum für Luft- und Raumfahrt (DLR), Berlin, Germany

Abstract We investigated mid-infrared reflectance spectra of anorthosite samples from Mt. Briand near the Manicouagan impact structure. Microprobe analyses of the plagioclase minerals reveal that they have a similar chemical composition (labradoritic), which is corroborated by the location of the Christiansen Feature at around 7.96 μm (1256 cm^{-1}). However, their respective spectral shapes differ from each other in the region of the reststrahlen bands. This is linked to the degree of Al,Si order within the plagioclase minerals, which also correlates with the previously assumed distance of the sample site to the impact melt. Powdering and sieving led to remarkable changes in the spectra resulting from different mechanical stability of minerals contained in the sample. Our data show that even very weakly shocked (6–10 GPa, shockstage S2) anorthosites could show spectra of Al,Si disordered plagioclase which we attribute to post shock heating after the impact shock. Consequently, the degree of Al,Si order has to be taken into account in the interpretation of remote sensing data. A comparison of synthetic linear mixture with an average Mercury spectrum reveals the possible presence of more or less anorthositic material with reduced degree of Al,Si order of the plagioclase component on Mercury's surface. The results of our study are helpful for the interpretation of data returned by space missions, especially for MERTIS - an infrared spectrometer on its way to Mercury.

Plain Language Summary The studied rocks, which contain predominantly the feldspar mineral plagioclase, are very common in our Solar System, for example, on the Moon and probably also on Mercury. The surface of planets without atmosphere, like Moon and Mercury are constantly the target of asteroid impacts. These impacts cause changes in the constituents of the rocks. The studied samples are from the area near a meteorite crater and show weak effects of the former meteorite impact. The infrared spectra of the samples have different shapes. This shape does not correlate with the chemical composition, but with the distribution of aluminum and silicon ions in the plagioclase components of the investigated samples. This distribution is often underestimated in remote sensing. Our study shows that this distribution of these ions is related to a previously assumed distance of the sample location from the impact. The results are useful for interpreting remote sensing data coming back from space missions. In our case, in particular, from an infrared spectrometer on its way to the planet Mercury called MERTIS. The study also presents a spectrum calculated from various mineral spectra comparable to the samples analyzed. This spectrum shows similarities to an average Mercury surface spectrum and suggests that the feldspars on the Mercury surface have a very disordered ion distribution.

1. Introduction

Anorthosites are plutonic rocks like diorites and gabbros, with a plagioclase content of > 90% but with minor mafic mineral phases (e.g., pyroxenes) of less than 10% (Le Maitre, 2002). Plagioclases are the solid solution between a Na-endmember ($NaAlSi_3O_8$/Ab) and a Ca-endmemeber ($CaAl_2Si_2O_8$/An). Plagioclases can also contain some potassium ($KAlSi_3O_8$/Or). In addition to the chemical composition, plagioclases are characterized by their degree of Al,Si order. The term *low plagioclase* indicate crystals with high Al,Si order and *high plagioclase* indicate crystals with low Al,Si order (Ribbe, 1983). A change of the Al,Si order does not change the chemical composition. However, both properties, chemical composition as well as Al,Si order,

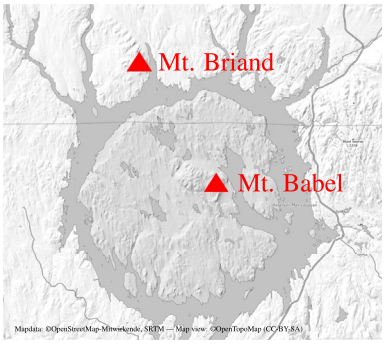

Figure 1. Relief overview of the Manicouagan impact structure with Mt. Babel and the location of sampling site outside the crater at Mt. Briand which is located in anorthositic bedrock (e.g., Grieve & Floran, 1978).

affect the shape of the mid-infrared (mid-IR) reflectance spectra (Reitze et al., 2020, 2021). On the surfaces of planetary objects without atmosphere, space weathering (large meteorite impacts, micrometeorite bombardment, as well as radiation originating from the Sun and the Galaxy) plays an important role (e.g., Bennett et al., 2013, and references therein). Shock experiments showed that spectra of plagioclases and anorthosites tend to lose mid-IR bands corresponding with the shock pressure (e.g., Johnson, 2012; Johnson et al., 2003; Jaret, Johnson, et al., 2018). Similar changes in the mid-IR plagioclase spectra occur in natural and synthetic samples that have a reduced degree of Al,Si ordering, but whose origin is not shock but temperature induced (Reitze et al., 2021). Without any shock, the Al,Si distribution is depended on the temperature for a given chemical composition (Ribbe, 1983). These spectra could therefore be misinterpreted as shocked plagioclases in the mid-IR. Investigations of the plagioclases from the Lappajärvi crater, Finland, revealed an almost highest possible degree of disorder, showing a complex interaction of shock and the impact melt (Bischoff & Stöffler, 1984). Simulated micrometeorite bombardment with laser irradiation of powder pressed pellets leads to a decrease of spectral contrast of the Reststrahlen bands (RBs) of plagioclase feldspar samples and a formation of smaller grain sizes due to a gardening process, which disturbs the flat surface of the pellets (Moroz et al., 2014; Weber et al., 2020).

The strongly eroded Manicouagan crater, Canada, is around 60 km in diameter with a central peak (Mt. Babel) and is located in Precambrian gneises (Dworak, 1969). Its age was determined with different methods to approximately 215.4 Ma (Jaret, Hemming, et al., 2018). Plagioclases of Mt. Babel are highly disordered with respect to their Al,Si distribution and sometimes converted into diaplectic glass, whereas plagioclase samples from Mt. Briand which is located north-northwest outside the crater (Figure 1), showed a greater degree of order (Dworak, 1969; van Soest et al., 2011).

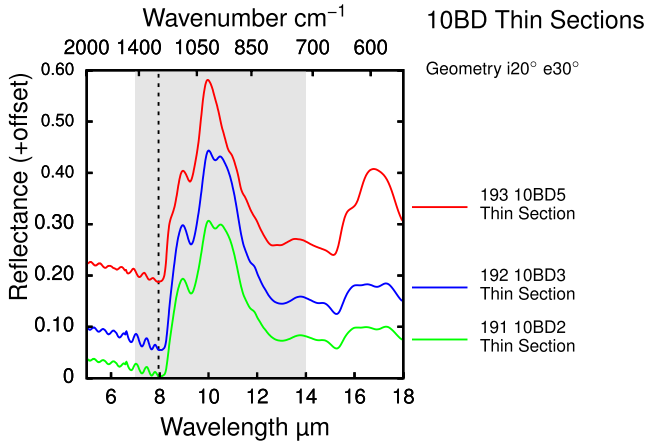

Figure 2. Thin section spectra of the three bulk rock samples. The measuring range of MErcury Radiometer and Thermal Infrared Spectrometer is indicated by the gray background between 7 and 14 µm (1,429 cm^{-1} and 714 cm^{-1}). The mean Christiansen Feature (CF) is around 7.95 µm (1,258 cm^{-1}) indicated by the black dotted line. The reststrahlen bands of the 10BD3 and 10BD2 sample are relatively similar with three clear peaks whereas the spectrum of the 10BD5 sample only show two clear peaks. Below the CF the spectra show an often observed *oscillating feature* of thin section spectra probably originated from the highly reflecting surface.

Besides Earth, where feldspars make up the most prominent mineral in the crust, plagioclases are especially widely distributed on the Moon (e.g., Wood et al., 1970). Mercury's surface is also thought to be composed of plagioclase-rich material (e.g., Evans et al., 2012; Nittler et al., 2011; Sprague et al., 1997; Vander Kaaden et al, 2017).

In October 2018, the BepiColombo spacecraft was launched to investigate Mercury. Onboard the spacecraft is the MErcury Radiometer and Thermal Infrared Spectrometer (MERTIS), which will explore Mercury's surface in the mid-IR (Hiesinger et al., 2010, 2020). The goals of MERTIS are studying and mapping the surface mineralogy as well as the thermal inertia (Hiesinger et al., 2010). For this, MERTIS measures in the wavelength region from 7 to 14 µm (1,429 cm^{-1} to 714 cm^{-1}) with 78 channels (Spectrometer Channels/TIS) and from 7 to 40 µm (1,429 cm^{-1} to 250 cm^{-1}) with 2 channels (Radiometer Channels/TIR) (Hiesinger et al., 2010, 2020).

In April 2020 a swing-by at the Earth-Moon system allowed MERTIS to study the Moon's surface from a distance of around 700,000 km. Because anorthosites are widely distributed on the Moon (e.g., Wood et al., 1970), knowledge of the mid-IR behavior of well characterized analogue samples of this rock type is essential for the correct interpretation of the acquired MERTIS spectra. In addition, mid-IR spectra of Mercury's surface will likely contain plagioclase-rich material. Thus a detailed comprehension of such material, its spectral behavior, and how different processes influences the spectra, is necessary for an accurate interpretation of the spectra. In the past, several mid-infrared studies investigated the mercu-

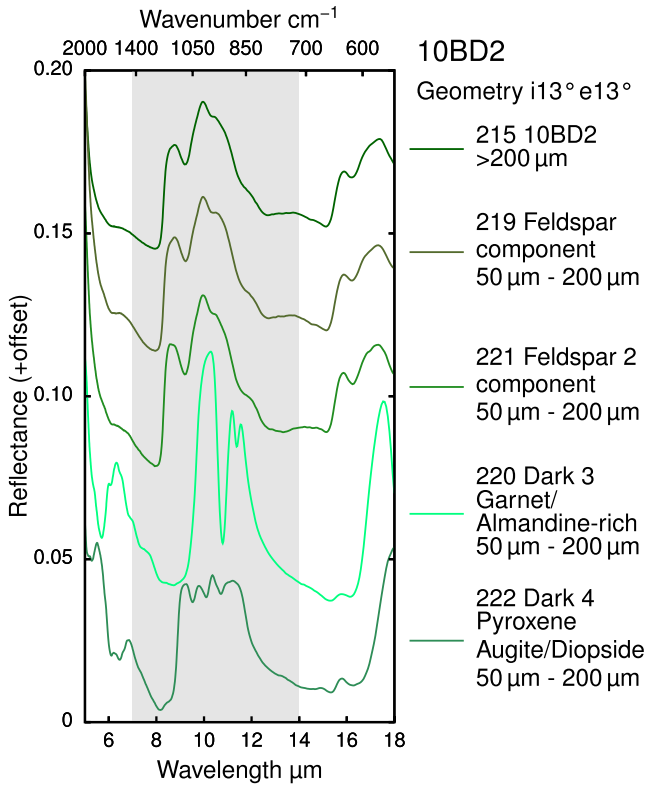

Figure 3. 10BD2 powder spectra of the original mineral separates taken from (Trieloff, 1993): bulk sample, two feldspar components, and two different dark phases. The bulk rock spectra is strongly affected by the feldspar component. The two spectra of the feldspar components differ only slightly from each other, especially the peak around 9 µm (1,111 cm^{-1}). The dark phases have no visual impact on the form of the bulk sample spectrum.

rian surface with Earth-based telescopes in order to determine the surface mineralogy (e.g., Sprague et al., 2009, and references therein). Some of these studies report feldspars (potassium feldspar and plagioclase feldspar) as potential rock forming minerals at Mercury's surface (e.g., Sprague et al., 1997, 2009). Furthermore, old surfaces of planets underwent numerous impacts, which affected the present minerals. Therefore, in this study our focus is on weakly shocked anorthosite samples as planetary surface analogue material. The spectra of the rock samples were analyzed due to effects which are caused by the properties of the minerals. This will help to distinguish between impact related effects and intrinsic structural related effects on the mineral spectra. In addition, we present a comparison of a telescopic hermean spectrum taken from Sprague et al. (2000) with synthetic spectral mixtures of material similar to the analyzed anorthosites.

2. Samples and Analyses

2.1. Sample Characterization

The analyzed rock samples 10BD2, 10BD3, and 10BD5 originating from Mt. Briand near the Manicouagan impact structure are reference samples of the dissertation by Trieloff (1993). The samples are very weakly shocked (maximum 6–10 GPa) anorthosites (Stöffler et al., 1991), which were used to determine the age of the Manicouagan event (Trieloff, 1993). Phase analysis of the thin sections of the anorthosites samples reveled a homogeneous distribution of the minerals, which were crystalline. Plagioclase is the most abounded phase with minimum 95%, followed by garnet (up to 5%), and small amounts of pyroxen and titanite (both < 1%). Some of the plagioclases show fractures and undulatory extinction. The handpieces were crushed and mineral separates were prepared by Trieloff (1993): One separate, which contains feldspar (two feldspar seperates for sample 10BD2, respectively) and two dark phases for sample 10BD2 (labeled Dark3 and Dark4) as well as three dark phases for samples 10BD3 (labeled Dark3, Dark4-, and Dark4+) and 10BD5 (labeled Dark1, Dark2, and Dark3). The bulk rock samples were sieved to grain size fractions of >200 µm, 100–200 µm, 60–100 µm, and <60 µm. The separates of feldspar have a mean grain size between 90 and 121 µm determined by light microscopy. We took one part of the feldspar mineral separates and sieved it in a fraction from 63 to 125 µm and a remaining fraction containing larger crystals. We reanalyzed the thin sections of the hand specimens to verify the mineralogical composition also via light microscopy. The thin sections of the three bulk rock samples were also analyzed with JEOL JXA-8530F Hyperprobe electron probe microanalyzer (EMPA) at Institut für Mineralogie (IfM) at the Westfälische Wilhelms-Universität (WWU) Münster with 15 kV acceleration voltage and a beam current of 15 nA and the usage of natural and synthetic standards to determine the chemical composition of the feldspar component (Jarsoewich et al., 1980).

2.2. Infrared

For the IR measurements, we took the powdered bulk rock samples and mineral separates prepared for Trieloff (1993). A Bruker 70v FTIR spectrometer with a liquid nitrogen cooled mercury cadmium telluride (MCT) detector was used for the mid-infrared reflectance measurements between 2 and 18 µm at the Infrared and Raman for Interplanetary Spectroscopy (IRIS) lab at the Institut für Planetologie at the WWU. The powder samples were measured with a grazing angle unit A513 which measures bi-conical reflectance with an incident angle of 20° and emergent angle of 30° (i20° e30°) and with an incident and emergent angle of 13° (i13° e13°). The thin sections of the bulk samples were also measured with the grazing angle

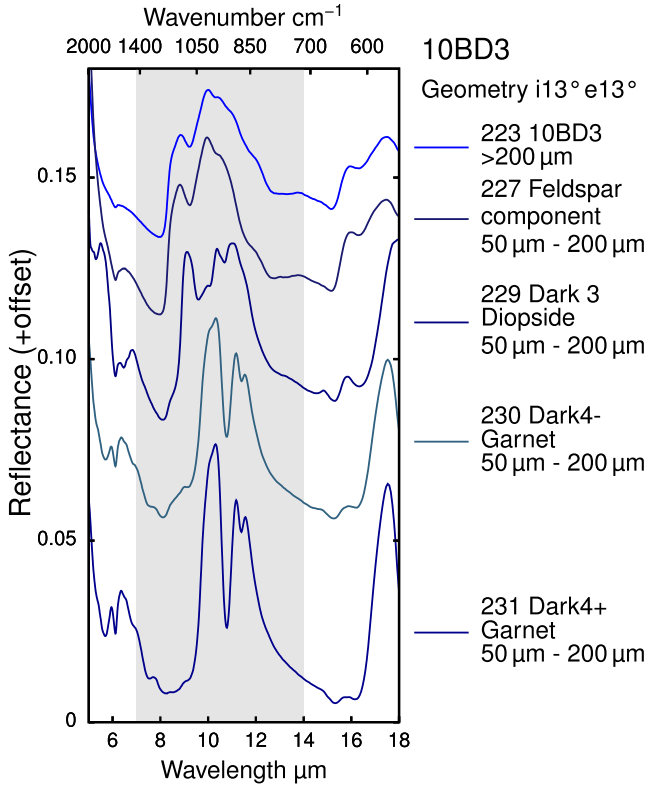

Figure 4. 10BD3 powder spectra of the original mineral separates taken from (Trieloff, 1993): bulk sample, feldspar component, and three different dark phases, where Dark4− and Dark4+ seem to be the same material. The bulk rock spectra is strongly affected by the feldspar component. The dark phases may influence the bulk sample spectrum in the range above 11 µm (909 cm^{-1}) where the slope of the bulk spectrum is shallower than in the pure feldspar spectrum.

unit at i20° e30°, which leads with the used 2 mm aperture to a spot size of 3.8–3.6 mm. All spectra were acquired in a vacuum of 2 hPa and room temperature (23°C to 25°C.) An INFRAGOLD™ rough gold standard was used for background calibration, for the thin sections, we used a polished gold mirror. The powder samples were placed in aluminum sample holders 1 cm in diameter with depths between 0.5 and 2 mm depending on the available amount of samples material and flattened with a spatula. Each single channel spectrum of sample and background were calculated through Fourier transformation of 512 single interferogram scans in double sided forward-backward scan mode. The reflectance was calculated as the ratio of sample single spectrum to background single channel spectrum ($I_{sample}/I_{reference}$).

Silicate minerals, especially feldspars, show distinct spectral features in the mid-infrared, RBs, due to stretching and bending of bonds between Si,Al, and O ions in the tetrahedrons which change their wavelength with chemical composition as well as state of Al,Si order (e.g., Iiishi et al., 1971). The Christiansen Feature (CF) at shorter wavelengths than the RBs is visible as a pronounced trough in reflectance spectra (peak in emissions spectra), which originates from a rapid change of the refractive index (Logan et al., 1973). Reflectance spectra of samples with a grain sizes below ~70 µm show the Transparency Feature (TF), which is a broad peak caused by stronger volume scattering compared to surface scattering (Pieters & Englert, 1993). A reduced grain size leads to a decreased overall reflectance and broader RB peaks (Pieters & Englert, 1993).

Autocorrelation analysis of infrared absorption spectra are widely used in mineralogy to determine several sample characteristics (e.g., Malcherek et al., 1995; Ballaran et al., 1999, for synthetic feldspars, and the chemical composition of garnets respectively). The autocorrelation technique is sensitive to the width of the analyzed peaks in the spectra. Reitze et al. (2020) and Reitze et al. (2021) used the autocorrelation method to analyze mid-IR reflectance spectra and were able to determine the degree of Al,Si order of alkali feldspars as well as plagioclase feldspars with the technique. The method uses the wavelength of the CF and the width of the spectral autocorrelation function between 7.27 and 12.11 µm (Reitze et al., 2021).

3. Results

Light microscopy and EMPA analyses on the thin sections showed that the samples 10BD2, 10BD3, and 10BD5 mostly contain plagioclase feldspar (10BD2 $Ab_{45}An_{52}Or_3$, 10BD3 $Ab_{46}An_{51}Or_3$, and 10BD5 $Ab_{49}An_{50}Or_1$; all labradoritic, Table 1). Minor phases in the samples are garnet, titanite, pyroxen, saussuritized plagioclase, alkali feldspar, and iron oxide.

We focused our analysis on infrared spectra from 7 to 14 µm, which is the measurement range of the MERTIS experiment. The following band positions were summed up in Table 1. The IDs refer to the IRIS spectral database, available at www.uni-muenster.de/Planetology (Weber et al., 2018).

3.1. Thin Sections

Figure 2 shows the spectra of the three bulk sample thin sections measured with i20;e30 geometry. The CF is at 7.97 µm (1,255 cm^{-1}) in the 10BD2 spectrum (ID 191), 7.98 µm (1,253 cm^{-1}) in the 10BD3 spectrum (ID 192), and 7.94 µm (1,260 cm^{-1}) in the 10BD5 spectrum (ID 193). The wavelength region of the RB is strongly affected by the feldspar within the samples. The spectra of samples ID 191 and ID 192 are relatively

Table 1
Electron Micropobe Data for the Feldspars Taken from the Three Samples and Important Feature Positions of Bulk Samples and the Corresponding Components

Sample	Oxides	wt-%	Std Dev	Cations	mol	Std Dev
10BD2	Na_2O	5.10	0.65	Na	1.34	0.17
	MgO	0.07	0.00	Mg	0.00	0.00
	Al_2O_3	28.81	1.06	Al	4.60	0.18
	SiO_2	54.65	1.42	Si	7.41	0.17
	K_2O	0.48	0.20	K	0.08	0.03
	CaO	10.63	1.13	Ca	1.54	0.17
	FeO	0.15	0.15	Fe	0.01	0.02
	TiO_2	0.00	0.00	Ti	0.00	0.00
	Cr_2O_3	0.00	0.00	Cr	0.00	0.00
	MnO	0.00	0.00	Mn	0.00	0.00
	Total	99.89		Total	15.00	
10BD3	Na_2O	5.14	0.17	Na	1.35	0.04
	MgO	0.07	0.02	Mg	0.00	0.00
	Al_2O_3	28.29	0.24	Al	4.53	0.02
	SiO_2	55.05	0.46	Si	7.48	0.02
	K_2O	0.48	0.08	K	0.08	0.01
	CaO	10.40	0.16	Ca	1.51	0.03
	FeO	0.13	0.04	Fe	0.01	0.01
	TiO_2	0.04	0.00	Ti	0.00	0.00
	Cr_2O_3	0.00	0.00	Cr	0.00	0.00
	MnO	0.02	0.00	Mn	0.00	0.00
	Total	99.61		Total	14.97	
10BD5	Na_2O	5.46	0.12	Na	1.44	0.03
	MgO	0.00	0.00	Mg	0.00	0.00
	Al_2O_3	28.41	0.27	Al	4.54	0.03
	SiO_2	55.10	0.30	Si	7.47	0.03
	K_2O	0.27	0.05	K	0.05	0.01
	CaO	10.26	0.19	Ca	1.49	0.02
	FeO	0.09	0.01	Fe	0.01	0.00
	TiO_2	0.00	0.00	Ti	0.00	0.00
	Cr_2O_3	0.00	0.00	Cr	0.00	0.00
	MnO	0.00	0.00	Mn	0.00	0.00
	Total	99.59		Total	15.00	

Table 1
Continued

Sample	ID	Type	CF	RB_1	RB_2	RB_3	RB_4	TF	Grain size
10BD2	191	Thin section	7.97	8.95	10.00	10.50			—
10BD3	192	Thin section	7.98	8.95	10.00	10.48			—
10BD5	193	Thin section	7.94	8.95	9.98				—
10BD2	215	Bulk Powder	7.96	8.76	9.96				> 200
	216	Bulk Powder	7.97	8.76	9.96				100–200
	217	Bulk Powder	8.00	8.76	9.96				60–100
	218	Bulk Powder	8.02	8.80	9.96		11.1[a]	12.14	< 60
	219	Fsp Powder	7.97	8.76	9.96	10.48[a]			50–200
	220	Dark3	8.73	10.29	11.18	11.54			50–100
	221	Fsp Powder	7.94	8.58	9.96	10.48[a]			50–100
	222	Dark4	8.16	9.25	9.79	10.36	11.21		50–100
10BD3	223	Bulk Powder	7.93	8.85	10.02				> 200
	227	Fsp Powder	8.00	8.83	9.96	10.48[a]			50–100
	229	Dark3	8.11	9.12	10.00	10.38	10.99		50–100
	230	Dark4−	8.11	10.31	11.18	11.54			50–100
	231	Dark4+	8.28	10.31	11.18	11.57			50–100
10BD5	232	Bulk Powder	7.94	8.95	9.92				> 200
	236	Fsp Powder	7.93	8.81	9.92				50–100
	237	Dark1	8.11	9.10	9.98	10.36	10.97		50–100
	238	Dark2	8.24	10.18	11.15	11.51			50–100
	239	Dark3	8.58	10.24	11.15	11.54			50–100

Note. Band positions and grain sizes in μm.
[a]Indicates a shoulder.

similar, but the ID 193 spectrum differs from the previous ones: All three samples show a clear RB peaks at ~8.95 μm (1,117 cm^{-1}). The spectra ID 191 and ID 192 have two further RB peaks at 10.00 μm (1,000 cm^{-1}) and 10.50 μm (952 cm^{-1}) in ID 191 and at 10.48 μm (954 cm^{-1}) in ID 192, respectively. In contrast, the ID 193 spectrum only contains one RB peak in this wavelength region at 9.98 μm (1,002 cm^{-1}).

3.2. Powder Samples

3.2.1. 10BD2

Figure 3 shows the spectra of 10BD2 powder samples, with bulk sample, feldspar components and dark phases. The whole rock spectrum (ID 215) is strongly affect by the feldspar component (ID 219). The CF is at 7.96 μm (1,256 cm^{-1}) in this spectrum (ID 215) compared to 7.97 μm (1,255 cm^{-1}) in the feldspar component 1 spectrum (ID 219) and 7.94 μm (1,260 cm^{-1}) in the feldspar component 2 spectrum (ID 221). The two feldspar spectra contain two large RBs, the stronger one at 9.96 μm (1,004 cm^{-1}) shows a strong shoulder at around 10.48 μm (954 cm^{-1}). In contrast, the weaker RB in the two feldspar spectra of sample 10BD2 shows a peak at 8.76 μm (1,142 cm^{-1}) in the ID 219 spectrum and a peak at 8.58 μm (1,166 cm^{-1}) in the ID 221 spectrum. Otherwise, the two feldspar components differ not significantly from each other. The two dark phases differ strongly from each other. The ID 220 spectrum contains one large RB peak at around 10 μm (1,000 cm^{-1}) and a double peak around 11 μm (909 cm^{-1}). The ID 222 spectrum contains four RB peaks between 9 μm (1,111 cm^{-1}) and 11 μm (909 cm^{-1}) each with similar intensity.

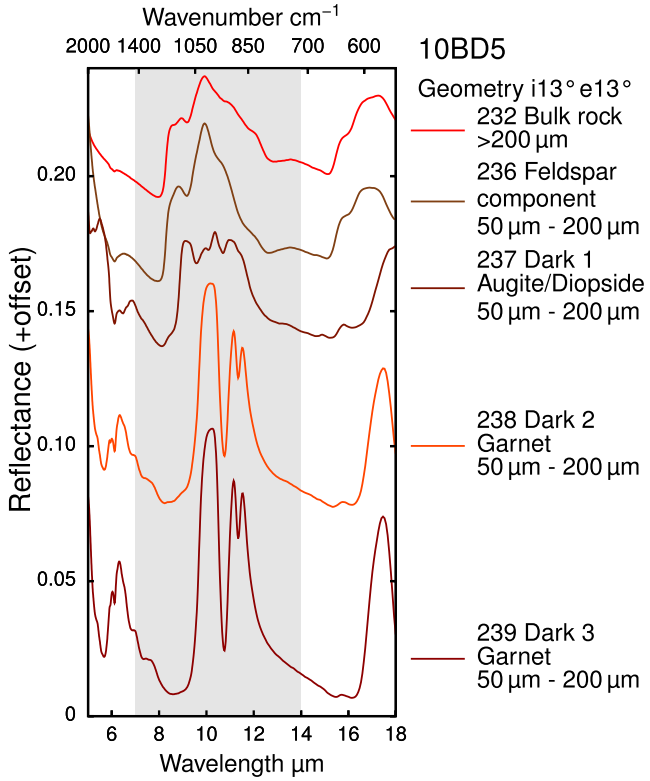

Figure 5. 10BD5 powder spectra of the original mineral separates taken from (Trieloff, 1993): bulk sample, feldspar component, and three different dark phases, where Dark 2 and Dark 3 seem to be the same material. The bulk rock spectra is strongly affected by the feldspar component. The dark phases may influence the bulk sample spectrum in the range above 11 µm (909 cm^{-1}) where the slope of the bulk spectrum is shallower than in the pure feldspar spectrum.

3.2.2. 10BD3

The spectra related with the sample 10BD3 are presented in Figure 4. The bulk rock spectrum ID 223 is also strongly influenced by the feldspar component (spectrum ID 227) and shows a CF at 7.93 µm (1,261 cm^{-1}) compared to 8.00 µm (1,250 cm^{-1}) in the feldspar spectrum. Nevertheless, the width of the RB region of the ID 223 spectrum is slightly larger than the pure feldspar spectrum. This may indicate an influence of the dark phase on the bulk rock spectrum. The feldspar spectrum ID 227 contains two RBs, one at 8.83 µm (1,133 cm^{-1}) and one at 9.96 µm (1,004 cm^{-1}) with a shoulder at around 10.48 µm (954 cm^{-1}). The spectra ID 230 and ID 231 (Dark phase 4+ and Dark phase 4−) are relatively similar showing three clear peaks at around 10.31 µm, 11.18 µm, and 11.54 µm (970 cm^{-1}, 895 cm^{-1}, and 867 cm^{-1}), whereas the spectrum ID 229 is clearly different, showing three clear peaks at 9.12 µm, 10.38 µm, and 10.99 µm (1,097 cm^{-1}, 963 cm^{-1}, and 910 cm^{-1}).

3.2.3. 10BD5

Figure 5 shows the spectra related with the 10BD5 sample. As before, the whole-rock powder sample spectrum (ID 232) is strongly affected by the feldspar component (spectrum ID 236). The CF is at 7.94 µm (1,260 cm^{-1}) in the bulk rock sample and at 7.93 µm (1,261 cm^{-1}) in the corresponding feldspar spectrum. The spectrum of the feldspar itself contains two RBs at 8.81 µm and at 9.92 µm (1,135 cm^{-1} and 1,008 cm^{-1}). The spectra of the dark phases are also very similar to the spectra of the dark phases of the 10BD3 sample.

3.2.4. The Effect of Sample Preparation

As expected, the powdered and sieved *bulk* rock samples (however, they are not the *bulk* rock samples anymore!) show changes not only due to grain size but also due to sample preparation. Figure 6 shows this for sample 10BD2. The CF of the 10BD2 bulk rock samples with a grain size TF 200 µm is at 7.96 µm (1,256 cm^{-1}) and shifts to 8.02 µm (1,247 cm^{-1}) in the fractions with grain sizes smaller than 60 µm. In addition to the strong plagioclase dominated RB at 9.96 µm (1,004 cm^{-1}) and shoulder at around 10.48 µm (954 cm^{-1}), a second shoulder appears in the spectrum of the finest fraction (ID 218) at around 11.1 µm (901 cm^{-1}) and a sharp peak at 12.14 µm (824 cm^{-1}) which is the TF.

4. Discussion

4.1. The Effect on Bulk Rock Spectra of Individual Mineral Components

The three infrared spectra of the weakly shocked anorthosite samples are highly affected by the plagioclase components. In contrast to this, the minerals which only make up a maximum of 10 vol% have only weak to no effects on the bulk sample spectrum of the largest grain size fraction. Only sample 10BD5 may be influenced by the dark mineral phases. Therefore, infrared remote sensing spectra of planetary surfaces containing anorthosites such as the Moon's highlands should show mostly the plagioclase signature.

The mineral separates containing the dark phases are most likely garnet (ID 220, 230, 231, 238, and 239) and pyroxene (ID 222, 229, and 237). The pyroxene component is a high Ca-pyroxene (e.g., Weber et al., 2016). The garnet spectrum is comparable with almandine-rich absorption spectra (Ballaran et al., 1999), however the comparability of absorption and reflectance spectra is low.

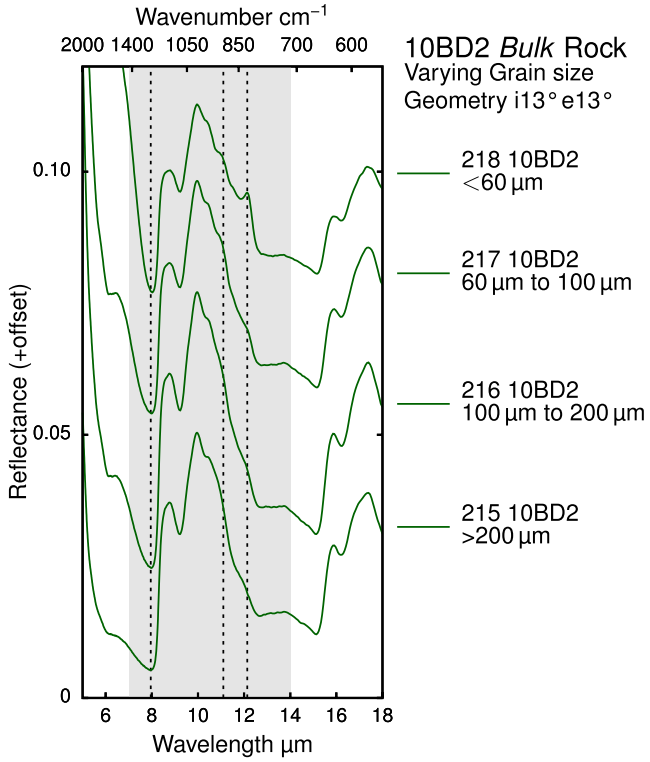

Figure 6. 10BD2 *bulk* rock, crushed and sieved to different grain size fractions. The spectral shape and wavelength of the CF is strongly affected by different mineral proportions within the samples because of different mechanical stability of the different minerals within the sample.

The samples are a good analogue for parts of Mercury's surface, because deconvolution of Earth-based infrared spectra of Mercury showed, besides a plagioclase component at some areas, accessory phases like pyroxene and garnet as possible constituents (Sprague et al., 2009).

4.2. Effects of Al,Si Order

Figure 7 shows a comparison of the feldspars prepared from the samples with four different plagioclase feldspars taken from the IRIS database. Sample ID 167 is a highly disordered pure albite (Reitze et al., 2020, 2021), sample ID 127 is a synthetic plagioclase with a ~ labradoritic composition, with or near to highest possible disorder, sample ID 2 is a natural low plagioclase with An_{53}, and sample ID 126 a synthetic anorthite (Reitze et al., 2021). ID 2 and ID 127 have a comparable An-content as the feldspars taken from the 10BD-samples (mean ~ $Ab_{47}An_{51}Or_2$). The spectral differences between ID 2 and ID 127 are due to the different degree of Al,Si order (Reitze et al., 2021). The wavelength of the CF is only affected by the chemical composition of the plagioclases and the environmental conditions (e.g., Conel, 1970; Donaldson Hanna et al., 2012; Nash & Salisbury, 1991) but the exact correlation function is debatable (Reitze et al., 2021). We are observing that the samples measured with our setup produces comparable results for the CF wavelengths for natural and synthetic samples of comparable composition. The RB at 8.75 µm (1,143 cm^{-1}) is related with Si-O stretching (Iiishi et al., 1971) and is observable in the plagioclase samples taken from the IRIS database, too. The RB at 9.95 µm (1,005 cm^{-1}) (Si(Al)-O stretching, Iiishi et al., 1971) is best matched with the spectra of samples ID 2 and ID 127, indicating a labradoritic composition. Nevertheless, also the high albite spectrum (ID 167) contains a strong RB peak in that wavelength region only slightly shifted two shorter wavelengths indicating that careful spectral comparison is necessary. The shoulder in the 10BD feldspar spectra is at around 10.48 µm (954 cm^{-1}) and related to Si(Al)-O stretching (Iiishi et al., 1971). It corresponds with a peak in the low plagioclase spectrum ID 2 and with a shoulder in the spectrum of sample ID 127. This shoulder corresponds with the most intensive RB in the An_{100} sample (ID 126), although, slightly shifted to longer wavelengths. These observations hint, that the plagioclases in the 10BD samples are disordered with respect to their Al,Si distribution. Applying the method derived in Reitze et al. (2021) to determine the degree of Al,Si order of plagioclase samples based on mid-IR reflectance data, the feldspars taken from 10BD2, ID 219 and ID 221, have a degree of Al,Si order of 0.37 and 0.27, respectively (mean 0.32). The feldspar taken from 10BD3 (ID 227) has an Al,Si degree of order of 0.30. The sample ID 236 taken from 10BD5 has an degree of order of 0.44 and is therefore the most ordered one. The range of possible degree of Al,Si order for plagioclase samples with ~ An_{50} is from approximately 0.12 to 0.45 (e.g., Kroll & Ribbe, 1980).

4.3. Implications of the Formation History of the Feldspars

Plutonic rocks like our anorthosites from Mt. Briand are characterized by slow cooling allowing to form a high degree of Al,Si order in the plagioclase. Shock experiments with shock pressures up to 45 GPa by Ostertag and Stöffler (1982) showed that the Al,Si distribution of feldspars remained unchanged due to a shock. However, short heating up to 100 h of these experimentally shocked samples lead to a fast loss of Al,Si order (Ostertag & Stöffler, 1982). This fast change of the Al,Si distribution was attributed to an enhanced Al,Si diffusion in shocked feldspars (Ostertag & Stöffler, 1982). In addition, the diffusion of the cations K, Na, and Ca were also strongly enhanced (Ostertag & Stöffler, 1982). Furthermore, just like extremely high shocked plagioclases (e.g., Jaret, Johnson, et al., 2018), the state of Al,Si order has a very large influence on the mean-IR spectra of plagioclases (Reitze et al., 2020, 2021). This means, disordered samples could easily be misinterpreted for shocked samples in mid-IR spectra. Our samples 10BD2, 10BD3, and 10BD5 are only

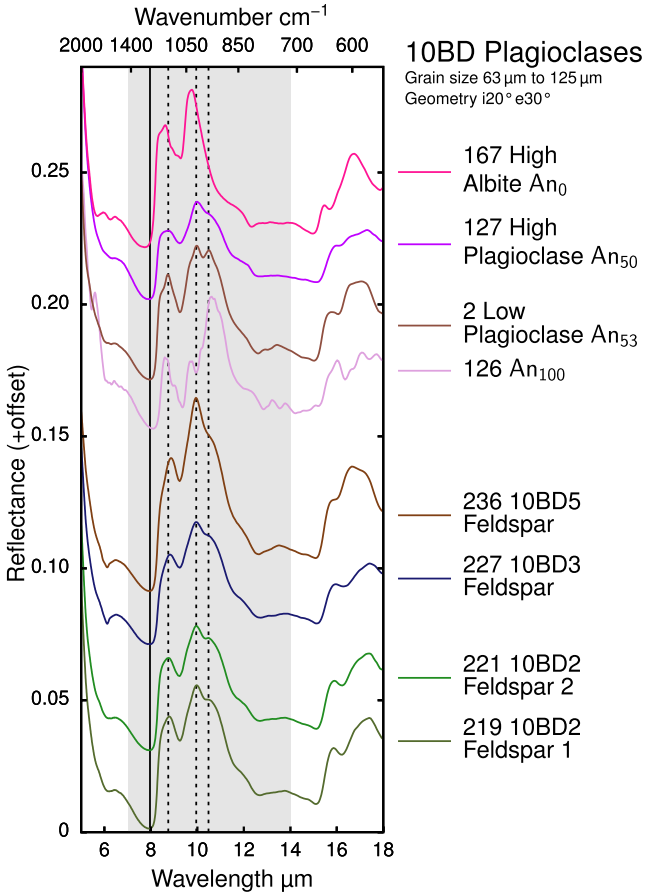

Figure 7. Comparison of the feldspar separates taken from the 10BD samples with four selected plagioclase samples: Pure high albite, a synthetic high plagioclase with ~ An_{50} (labradorite), a natural low plagioclase with ~ An_{53}, and a synthetic pure anorthite. The black line indicates the mean wavelength of the feature taken from the four feldspars taken from the 10BD samples. The three dotted lines indicate the mean wavelength of the two reststrahlen bands visible in the 10BD feldspar spectra and the position of one shoulder. The feldspars of the 10BD samples best match with the high plagioclase with labradoritic composition.

very weakly shocked and the shock wave temperature achieve a value of 20°C to 50°C (Trieloff, 1993). Since there is no evidence of higher shock in our samples originating from the plutonic bedrock outside the crater from Mt. Briand, such as planar deformation lamellae, increased birefringence or even amorphous regions (Jaret, Johnson, et al., 2018; Stöffler et al., 1991), we assume that the Al,Si distribution of the feldspars was altered by the heat transferred outside, which was provided by the impact melt, after the impact. Moreover, the samples with the highest disorder experienced the longest time (80 h) of a temperature of around 1,100°C after the impact (Trieloff, 1993). The sample with a mean degree of order experienced an intermediate time (50 h) of such high temperatures and the ordered one experienced only 8 h (Trieloff, 1993). These time-temperature-correlations were calculated by Trieloff (1993) using the Ar-Ar-data and were interpreted in terms of distance (not necessarily into the depth) between the impact melt and the location of the samples. Therefore, this observation is important for the interpretation of the remotely acquired mid-IR spectra of atmosphereless planetary surfaces: It must be considered that even weakly shocked anorthosites can have a reduced degree of order within their plagioclase components without the formation of devitrified diaplectic or fusion formed glass, which leads consequently to spectra dominated by high plagioclases. This is especially important for the MERTIS observations of Mercury and the heavily cratered highlands of the Moon.

The spectral changes associated with crushing and sieving are related to the different original sizes and the mechanical stability of the various minerals within the rock sample. The plagioclase crystals in the anorthosites are larger than the dark phases and break up later during pulverization. Sieving such an anorthosite sample leads to a different mineral composition in the different grain size fractions. Therefore, the *bulk* rock samples are richer in dark phases and therefore the spectra are more influenced by the dark phases. Vice versa, the grain size separates with smaller sizes contain less of the dark phases, which was already shown for lunar mare soils by Taylor et al. (2001). This process has to be considered when studying laboratory analogue material but also for real planetary surfaces. If a rock is composed of different minerals, each of which exhibiting different mechanically stabilities and weathering properties, meteoroid bombardment can become a mineral-specific break-up process. Because there is no sieving on the planetary surfaces, the more stable mineral will influence the spectra more in the region of the RB because the other one is finer and spectra of finer separates do not show as clear RB as the coarser ones (e.g., Pieters & Englert, 1993; Moroz et al., 2014). On the other hand, the TF should be than more influenced by the mechanically weaker mineral. The TF observed in the spectrum of the finest fraction of 10BD2 *bulk* rock sample (ID 218, Figure 6) is similar to the TF peak in the spectrum of the finest grain size (<25 µm) of sample ID 127 at 12.17 µm (822 cm^{-1}) also reflecting the low degree of Al,Si order (Reitze et al., 2021). However, this conclusion will only be true for a homogeneous distribution of the different particles of the regolith and not, if the fine fraction clinging to the larger particles mimicking a very fine grained surface. Nevertheless, observation of the Moon and it's relatively well known regolith in the mid-infrared may support this thesis.

4.4. Comparison to Hermean Spectrum

Figure 8 shows an average Mercury telescopic-gained emissivity spectrum taken from Sprague et al. (2000), in a first step turned in reflectance with Kirchhoff's law, and the same spectrum with a baseline fit, in

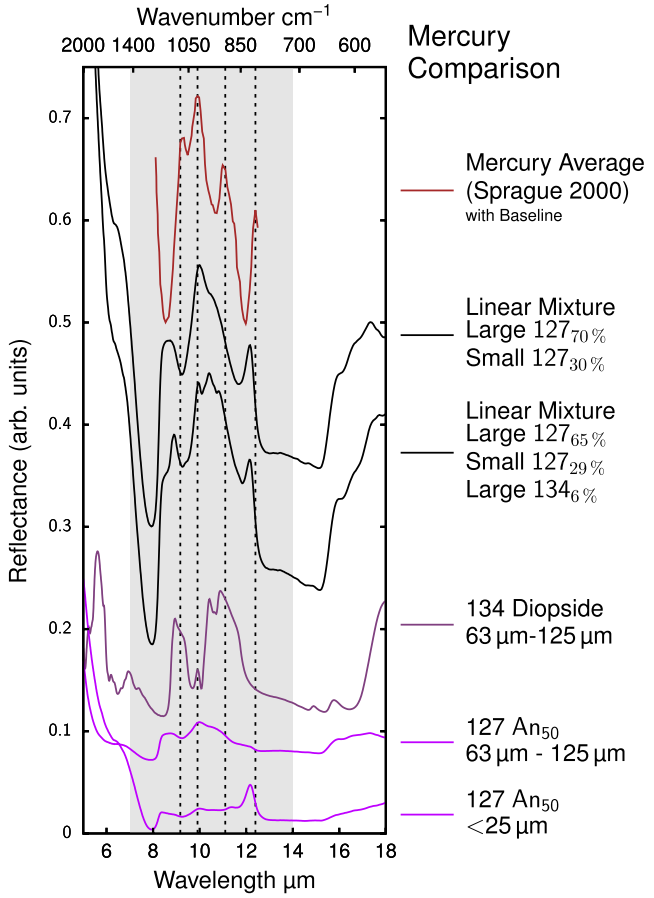

Figure 8. From top to bottom: (Spectrum 1) Average Mercury spectrum taken from (Sprague et al., 2000, turned into reflectance with Kirchhoff's law), normalized with a baseline (see also Weber et al., 2016, Figure 14). (Spectrum 2) Synthetic linear mixture of the feldspar spectrum of sample ID 127 with two different grain sizes scaled to increase contrast, (Spectrum 3) Synthetic linear mixture of two spectra with the same grain size fractions of ID 127 as before and ID 134 diopside scaled to increase contrast, (Spectrum 4) diopside ID 134 with a grain size between 63 and 125 µm, (Spectrum 5, ID 127), synthetic high labradorite with a grain size between 63 and 125 µm, and (Spectrum 6) with grain sizes smaller 25 µm. The four main features in the average Mercury spectrum marked with black dashed lines match relatively well with features contained in the linear mixture spectrum while the intensity of the ~11 µm bands is not well resolved.

comparison with our data. This spectrum contains four sharp peaks at 9.12 µm, 9.91 µm, and 11.1 µm. Spectra of feldspars with reduced degree of Al,Si order also contain clear peaks in that range at slightly below 9 µm and around 10 µm (e.g., ID 127 or ID 227 grain size 63–125 µm). The spectrum of a fine grained (<25 µm) high plagioclase (e.g., ID 127) shows a strong TF at 12.17 µm. Therefore, we calculated in a second step a simple linear mixture of a high plagioclase with a grain size ranging from 63 to 125 µm and with a grain size smaller 25 µm (Spectrum 3 from top of Figure 6). In this synthetic mixture spectrum, the peaks around 9 µm, 10 µm, and 12.4 µm are present but slightly shifted. Only the peak at 11.1 µm, which is visible in the Mercury spectrum is missing. Hence, in a third step, we added a diopside spectrum (ID 134 grain size 63–125 µm) to the mixed spectrum (Spectrum 4 from top of Figure 8). The shown mixture is composed of 65% of ID 127 with the larger grain size, 29% of ID 127 with the smallest grain size, and 6% of ID 134. This linear mixture spectrum shows features at comparable wavelengths than the baselined average Mercury spectrum, especially the 12.40 µm feature is now present resulting from TF of the fine-grained high plagioclase component. In addition, there is now a peak at around 10.41 µm resulting from the pyroxene component.

This simple comparison of a Mercury spectrum and our laboratory data reveals, that Mercury's surface can be interpreted as ~anorthositic in certain areas, where the plagioclase component is ~labradoritic in composition, which is an agreement with earlier studies (e.g., Sprague et al., 1997). In addition, we can assume, that the plagioclase component has a reduced degree of Al,Si order. As expected for a space weathered surface, the present material has fine-grained components composed of the main present mineral indicated by the TF at 12.4 µm. Nevertheless, the fine-grained component in the linear mixture is only minor compared to the larger components, which is in agreement with mature regolith material from the Moon, where larger particles between 16 mm and around 62 µm make up of approximately 70% of the regolith (McKay et al., 1974). The small deviation between the wavelength of the feature observed in the Mercury and the calculated spectra is probably due to the slightly different chemical compositions (Reitze et al., 2020). The interpretation that the TF reflects the plagioclase component is consistent with the previously discussed mechanical stability of the various minerals in a rock. Therefore, the pyroxene component in the linear mixture is probably over-estimated because of its stability (Moroz et al., 2014; Weber et al., 2020). The non-fitting peak arising from the pyroxene component is probably an artifact of the availability of a pyroxene spectrum, which correctly matches the characteristics of the pyroxenes present at Mercury in terms of chemical composition and crystallographic properties (Putnis, 1992). The local reflectance low may be interpreted as CF, but could be an artifact of the baseline calibration, thermal gradients in Mercury's surface regolith (e.g., Donaldson Hanna et al., 2012), or the difficult temperature calibration of the emissivity spectra of the large surface area probed at Mercury. The observation of a reduced degree of Al,Si order is, to our knowledge, discussed for Mercury's surface spectra for the first time. There are two possible explanations for this observation: (a) The plagioclases crystallized in a magma, which flowed out preserving the observed degree of Al,Si order. (b) The plagioclases were shocked by an impact event combined by a post shock heating event lead to the reduced degree of Al,Si order (e.g., Bischoff & Stöffler, 1984). These two mechanisms may act together or separate from each other. This reveals the chance of interpreting the infrared spectra of Mercury and other planetary bodies in terms of (thermal) formation history and shows the importance of databases including well-characterized analog spectra.

5. Conclusion

We analyzed weakly shocked anorthosite samples from Mt. Briand near the Manicouagan impact structure. The bulk sample spectra were strongly affected by the plagioclase components indicating that remote sensing of such anorthosites in the mid-infrared will also show mostly the feldspar signature. The dark and opaque phases (mostly pyroxene, garnet, and titanite) do not significantly affect the spectral shape of the largest grain size fraction but become more important for the smallest grain size fraction because of accumulation effects by sieving due to the mineral stability. This effect is partly also important for remote sensing in the mid-infrared. Mechanically more stable minerals may accumulate in the regolith as larger grains than less stable ones, mimicking a higher content of the stable phases. Analyses of feldspar mineral separates prepared from the bulk samples, all with labradoritic composition, revealed that the spectra are more comparable with high plagioclases (lower degree of Al,Si order) than with low plagioclases (higher degree of Al,Si order) with labradoritic composition. From our observations, it appears that the impact melt of the Manicouagan impact is responsible for the observed reduced degree of order of the plagioclases at Mt. Briand outside the crater. The shock wave of the impact has first disturbed the plagioclase mineral structure and the temperature increase induced by the heat, which was conducted from the impact melt, leads to our findings, which also correlate with the time span the host rock was heated to 1,100°C through the impact melt reported by Trieloff (1993). The degree of order is lower in the samples, which were hotter for longer times. This result is important for the interpretation of remotely acquired mid-IR spectra of planetary surfaces, which are covered by large impacts. Therefore, plagioclase-rich rocks, which were not in direct contact with an impact crater and therefore only weakly shocked may nevertheless show spectra of high plagioclases because of a short heating event.

The comparison of a Mercury spectrum and a synthetic linear mixture of high plagioclase and pyroxene shows, that Mercury's surface is probably composed of anorthosites, in which the plagioclases are more or less labradoritic in composition and with a degree of Al,Si order between the most possible ordered and most possible disordered. The work reveals, that a very precise and comprehensive sample characterization of laboratory analogue material is indispensable for correct interpretations of remote sensing data and can hint to the formation history of the observed surfaces or samples.

Data Availability Statement

The spectra are available in the IRIS spectral database at https://www.uni-muenster.de/Planetology/en/ifp/ausstattung/iris_spectra_database.html (Weber et al., 2018).

Acknowledgments
The used anorthosite samples were kindly provided by Mario Trieloff (Heidelberg). This work is partly supported by the DLR funding 50 QW 1701 in the framework of the BepiColombo mission. We gratefully acknowledge the helpful comments of the editor Deanne Rogers and the reviewers Steven Jaret and Paul Lucey, which significantly improved the manuscript. Open access funding enabled and organized by Projekt DEAL.

References

Ballaran, T., Carpenter, M., Geiger, C., & Koziol, A. (1999). Local structural heterogeneity in garnet solid solutions. *Physics and Chemistry of Minerals*, *26*(7), 554–569. https://doi.org/10.1007/s002690050219

Bennett, C. J., Pirim, C., & Orlando, T. M. (2013). Space-weathering of solar system bodies: A laboratory perspective. *Chemical Reviews*, *113*(12), 9086–9150. https://doi.org/10.1021/cr400153k

Bischoff, A., & Stöffler, D. (1984). Chemical and structural changes induced by thermal annealing of shocked feldspar inclusions in impact melt rocks from Lappajarvi crater, Finland. *Lunar and Planetary Science Conference Proceedings*, *89*, B645–B656. https://doi.org/10.1029/JB089iS02p0B645

Conel, J. (1970). A new method for determining abundance in silicate glass from powder film transmission measurements. In *Space programs summary 37–63, vol. iii. supporting research and advanced development*. Jet Propulsion Laboratory.

Donaldson Hanna, K. L., Thomas, I. R., Bowles, N. E., Greenhagen, B. T., Pieters, C. M., Mustard, J. F., & Wyatt, M. B. (2012). Laboratory emissivity measurements of the plagioclase solid solution series under varying environmental conditions. *Journal of Geophysical Research*, *117*, E11004. https://doi.org/10.1029/2012je004184

Dworak, U. (1969) Stoßwellenmetamorphose des Anorthosits vom Manicouagan Krater, Québec, Canada. *Contributions to Mineralogy and Petrology*, *24*(4), 306–347. https://doi.org/10.1007/BF00371273

Evans, L. G., Peplowski, P. N., Rhodes, E. A., Lawrence, D. J., McCoy, T. J., Nittler, L. R., & Goldsten, J. O. (2012). Major-element abundances on the surface of Mercury: Results from the MESSENGER gamma-ray spectrometer. *Journal of Geophysical Research*, *117*, E00L07. https://doi.org/10.1029/2012JE004178

Grieve, R. A. F., & Floran, R. J. (1978). Manicouagan impact melt, Quebec 2. Chemical interrelations with basement and formational processes. *Journal of Geophysical Research*, *83*(B6), 2761–2771. https://doi.org/10.1029/JB083iB06p02761

Hiesinger, H., Helbert, J., Alemanno, G., Bauch, K. E., D'Amore, M., Maturilli, A., & Mertis Co-I Team (2020). Studying the composition and mineralogy of the Hermean surface with the Mercury Radiometer and Thermal Infrared Spectrometer (MERTIS) for the BepiColombo Mission: An update. *Space Science Reviews*, *216*(6), 110. https://doi.org/10.1007/s11214-020-00732-4

Hiesinger, H., Helbert, J., & MERTIS Co-I Team (2010). The Mercury Radiometer and Thermal Infrared Spectrometer (MERTIS) for the BepiColombo mission. *Planetary and Space Science*, *58*, 144–165. https://doi.org/10.1016/j.pss.2008.09.019

Iiishi, K., Tomisaka, T., Kato, T., & Umegaki, Y. (1971). Isomorphous substitution and infrared and far infrared spectra of the feldspar group. *Neues Jahrbuch für Mineralogie Abhandlungen*, *115*, 98–119.

Jaret, S., Hemming, S. R., Rasbury, E. T., Thompson, L. M., Glotch, T. D., Ramezani, J., & Spray, J. G. (2018). Context matters – Ar–Ar results from in and around the manicouagan impact structure, Canada: Implications for Martian meteorite chronology. *Earth and Planetary Science Letters*, *501*, 78–89. https://doi.org/10.1016/j.epsl.2018.08.016

Jaret, S., Johnson, J. R., Sims, M., DiFrancesco, N., & Glotch, T. (2018). Microspectroscopic and petrographic comparison of experimentally shocked albite, andesine, and bytownite. *Journal of Geophysical Research: Planets*, *123*(7), 1701–1722. https://doi.org/10.1029/2018JE005523

Jarsoewich, E., Nelen, J., & Norberg, J. A. (1980). Reference samples for electron microprobe analysis. *Geostandards Newsletter*, *4*(1), 43–47. https://doi.org/10.1111/j.1751-908X.1980.tb00273.x

Johnson, J. R. (2012). Thermal infrared spectra of experimentally shocked andesine anorthosite. *Icarus*, *221*, 359–364. https://doi.org/10.1016/j.icarus.2012.08.012

Johnson, J. R., Hörz, F., & Staid, M. (2003). Thermal infrared spectroscopy and modeling of experimentally shocked plagioclase feldspars. *American Mineralogist*, *88*(10), 1575–1582. https://doi.org/10.2138/am-2003-1020

Kroll, H., & Ribbe, P. H. (1980). Determinative diagrams for Al,Si order in plagioclases. *American Mineralogist*, *65*, 449–457.

Le Maitre, R. (Ed.), (2002). *Igneous rocks: A classification and glossary of terms: Recommendations of the international union of geological sciences subcommission on the systematics of igneous rocks* (2nd ed.). Cambridge University Press. https://doi.org/10.1017/CBO9780511535581

Logan, L. M., Hunt, G. R., Salisbury, J. W., & Balsamo, S. R. (1973). Compositional implications of Christiansen frequency maximums for infrared remote sensing applications. *Journal of Geophysical Research*, *78*(23), 4983–5003. https://doi.org/10.1029/JB078i023p04983

Malcherek, T., Kroll, H., Schleiter, M., & Salje, E. K. H. (1995). The kinetics of the monoclinic to monoclinic phase transition in $BaAl_2Ge_2O_8$-feldspar. *Phase Transitions*, *55*(1–4), 199–215. https://doi.org/10.1080/01411599508200434

McKay, D. S., Fruland, R. M., & Heiken, G. H. (1974). Grain size and the evolution of lunar soils. *Lunar and Planetary Science Conference Proceedings*, *1*, 887–906.

Moroz, L. V., Starukhina, L. V., Rout, S. S., Sasaki, S., Helbert, J., Baither, D., & Hiesinger, H. (2014). Space weathering of silicate regoliths with various FeO contents: New insights from laser irradiation experiments and theoretical spectral simulations. *Icarus*, *235*, 187–206. https://doi.org/10.1016/j.icarus.2014.03.021

Nash, D. B., & Salisbury, J. W. (1991). Infrared reflectance spectra (2.2–15 μm) of plagioclase feldspars. *Geophysical Research Letters*, *18*(6), 1151–1154. https://doi.org/10.1029/91gl01008

Nittler, L. R., Starr, R. D., Weider, S. Z., McCoy, T. J., Boynton, W. V., Ebel, D. S., & Sprague, A. L. (2011). The major-element composition of Mercury's surface from MESSENGER X-ray spectrometry. *Science*, *333*, 1847–1850. https://doi.org/10.1126/science.1211567

Ostertag, R., & Stöffler, D. (1982). Thermal annealing of experimentally shocked feldspar crystals. *Lunar and Planetary Science Conference Proceedings*, *87*, 457–A464. https://doi.org/10.1029/JB087iS01p0A457

Pieters, C. M., & Englert, P. A. J. (Eds.), (1993). *Topics in remote sensing 4. Remote geochemical analysis: Elemental and mineralogical composition*. Cambridge University Press.

Putnis, A. (1992). *Introduction to mineral science*. Cambridge University Press.

Reitze, M. P., Weber, I., Kroll, H., Morlok, A., Hiesinger, H., & Helbert, J. (2020). Mid-infrared spectroscopy of alkali feldspar samples for space application. *Mineralogy and Petrology*, *114*(5), 453–463. https://doi.org/10.1007/s00710-020-00709-9}

Reitze, M. P., Weber, I., Morlok, A., Hiesinger, H., Bauch, K. E., Stojic, A. N., & Helbert, J. (2021). Mid-infrared spectroscopy of crystalline plagioclase feldspar samples with various Al,Si order and implications for remote sensing of mercury and other terrestrial solar system objects. *Earth and Planetary Science Letters*, *554*, 116697. https://doi.org/10.1016/j.epsl.2020.116697

Ribbe, P. H. (1983). *Feldspar mineralogy*. Berlin, Boston. De Gruyter.

Sprague, A. L., Deutsch, L. K., Hora, J., Fazio, G. G., Ludwig, B., Emery, J., & Hoffmann, W. F. (2000). Mid-infrared (8.1–12.5 μm) imaging of Mercury. *Icarus*, *147*(2), 421–432. https://doi.org/10.1006/icar.2000.6447

Sprague, A. L., Donaldson Hanna, K. L., Kozlowski, R. W. H., Helbert, J., Maturilli, A., Warell, J. B., & Hora, J. L. (2009). Spectral emissivity measurements of Mercury's surface indicate Mg- and Ca-rich mineralogy, K-spar, Na-rich plagioclase, rutile, with possible perovskite, and garnet. *Planetary and Space Science*, *57*, 364–383. https://doi.org/10.1016/j.pss.2009.01.006

Sprague, A. L., Nash, D. B., Witteborn, F., & Cruikshank, D. P. (1997). Mercury's feldspar connection - Mid-IR measurements suggest plagioclase. *Advances in Space Research*, *19*, 1507. https://doi.org/10.1016/s0273-1177(97)00363-3

Stöffler, D., Keil, K., & Edward, R. D. S. (1991). Shock metamorphism of ordinary chondrites. *Geochimica et Cosmochimica Acta*, *55*(12), 3845–3867. https://doi.org/10.1016/0016-7037(91)90078-J

Taylor, L. A., Pieters, C. M., Keller, L. P., Morris, R. V., & McKay, D. S. (2001). Lunar mare soils: Space weathering and the major effects of surface-correlated nanophase Fe. *Journal of Geophysical Research: Planets*, *106*(E11), 27985–27999. https://doi.org/10.1029/2000JE001402

Trieloff, M. (1993). *Datierung impaktmetamorpher Gesteine und methodische Ergänzungen zur 40 Ar-39 Ar-Altersbestimmungstechnik*. PhD thesis at Universität Heidelberg.

Vander Kaaden, K. E., McCubbin, F. M., Nittler, L. R., Peplowski, P. N., Weider, S. Z., Frank, E. A., & McCoy, T. J. (2017). Geochemistry, mineralogy, and petrology of boninitic and komatiitic rocks on the mercurian surface: Insights into the mercurian mantle. *Icarus*, *285*, 155–168. https://doi.org/10.1016/j.icarus.2016.11.041

van Soest, M. C., Hodges, K. V., Wartho, J.-A., Biren, M. B., Monteleone, B. D., Ramezani, J., & Thompson, L. M. (2011). (U-Th)/He dating of terrestrial impact structures: The manicouagan example. *Geochemistry, Geophysics, Geosystems*, *12*(5), Q0AA16. https://doi.org/10.1029/2010GC003465

Weber, I., Morlok, A., Bischoff, A., Hiesinger, H., Ward, D., Joy, K. H., & Münker, C. (2016). Cosmochemical and spectroscopic properties of Northwest Africa 7325—A consortium study. *Meteoritics & Planetary Sciences*, *51*(1), 3–30. https://doi.org/10.1111/maps.12586

Weber, I., Morlok, A., Grund, T., Bauch, K. E., Hiesinger, H., Stojic, A., & Joy, K. H. (2018). A mid-infrared reflectance database in preparation for space missions. In *Lunar and planetary science conference* (p. 1430).

Weber, I., Stojic, A. N., Morlok, A., Reitze, M. P., Markus, K., Hiesinger, H., & Helbert, J. (2020). Space weathering by simulated micrometeorite bombardment on natural olivine and pyroxene: A coordinated IR and TEM study. *Earth and Planetary Science Letters*, *530*, 115884. https://doi.org/10.1016/j.epsl.2019.115884

Wood, J. A., Dickey, J. S., Marvin, U. B., & Powell, B. N. (1970). Lunar Anorthosites. *Science*, *167*(3918), 602–604. https://doi.org/10.1126/science.167.3918.602